Numerical study of one-dimensional compression in granular materials

Numerical study of one-dimensional compression in granular materials

J. C. Lopera Perez[1], C. Y. Kwok[1], C. O'Sullivan[2], X. Huang[1, 2] & K. J. Hanley[2, 3]

[1]*Department of Civil Engineering, The University of Hong Kong, Haking Wong Building, Pokfulam Road, Hong Kong*

[2]*Department of Civil and Environmental Engineering, Imperial College London, Skempton Building, London SW7 2AZ, UK*

[3]*Institute for Infrastructure and Environment, School of Engineering, The University of Edinburgh, Edinburgh EH9 3JL, Scotland, UK*

Abstract

The Discrete Element Method (DEM) has been employed to simulate vertical one-dimensional compression of an idealized soil. Direct measurement of the full stress tensor was possible and the results show that K_0 (the ratio of horizontal to vertical effective stresses) increases with void ratio, which is consistent with previous experimental studies. The anisotropic fabric induced during compression was quantified by considering the orientations and magnitudes of the normal contact forces. For the denser samples there was a definite bias towards more vertically-oriented contacts, resulting in lower stresses being transmitted in the horizontal direction for a given vertical stress. In contrast, the contacts were oriented more isotropically in the looser samples, allowing more similar stresses to be transmitted in the horizontal and vertical directions.

Keywords: Discrete-element modelling; fabric/structure of soils; particle-scale behaviour

1. Introduction

The coefficient of lateral earth pressure at rest (K_0), defined as the ratio of horizontal effective stress (σ'_h) to vertical effective stress (σ'_v) measured under zero lateral strain conditions, is an important parameter used for the design of geotechnical structures. Measurement of horizontal effective stresses is non-trivial and so practising engineers tend to use the formula put forward by Jaky (1944), which correlates K_0 to the angle of shearing resistance:

$$K_0 = 1 - \sin \phi' \quad (1)$$

Where ϕ' is the effective angle of shearing resistance which is often taken as the angle of shearing resistance at the critical state (ϕ'_{cv}) (Jaky, 1944; Mesri & Hayat, 1993). This definition implies that there is a unique K_0 value for a given soil type and that K_0 is independent of initial state (i.e., packing density and stress level). The angle of shearing resistance at the peak stress (ϕ'_p) is sometimes used in equation (1) (Mesri & Vardhanabhuti, 2007; Talesnick, 2012; Lee *et al*, 2013). ϕ'_p depends on the material state (Been & Jefferies, 1985); thus if ϕ'_p is used in Equation (1), at a given stress level K_0 will increase with increasing void ratio. While Jaky's equation has been successfully applied in a large range of engineering applications, it may fail to predict the measured K_0 as it does not consider certain factors in the granular materials that may affect the K_0 value. K_0 experiments conducted by Chu & Gan (2004) and Wanatowski & Chu (2007) found relatively high K_0 values and a marked sensitivity of the K_0 response to the initial void ratio (e_0) for loose sand samples; for denser sands the K_0 values were lower and less sensitive to variations in packing density. Similar observations were reported by Okochi & Tatsuoka (1984), Mesri & Vardhanabhuti (2007), Northcutt & Wijewickreme (2013) and Lee *et al* (2013). In contrast, Talesnick (2012) reported higher K_0 values for dense states than for loose ones. It is worth mentioning that the differences in the experimental procedures, testing devices, sample preparation techniques and data acquisition methods between the studies likely influence any variation in the observed K_0 – void ratio dependency.

Differences in size, shape or roughness of particles also influence the measured K_0 values. Lee *et al* (2013) measured higher values of K_0 for non-etched glass beads than for etched glass beads. Furthermore, sub-angular and angular particles showed lower values of K_0 than glass beads. Changes in particle shape and hence in the connectivity of particles affect the fabric of granular materials which is closely related to the K_0 values (Guo & Stolle, 2006; Northcutt & Wijewickreme, 2013).

Lee *et al* (2013) attributed the low values obtained for K_0 of dense materials to the development of strong force chains in the vertical direction, leading to less stress transmission in the horizontal direction. However, Talesnick (2012) attributed the high K_0 values for dense materials to the dilatant

nature of dense soils: it is difficult to accept this explanation as dilation is suppressed during one-dimensional compression. This contribution aims to develop a science-based, fundamental understanding of the dependency of K_0 on void ratio. Discrete Element Method (DEM) simulations of one-dimensional compression tests were performed; the stresses could be directly calculated from the contact forces and so the vertical and horizontal stresses could be quantified accurately which is difficult to achieve in physical experiments.

2. DEM Simulations

This study used a modified version of the open-source code LAMMPS (Plimpton, 1995). Three-dimensional numerical samples were created as a representative volume element consisting of 22,312, initially non-contacting, spherical particles enclosed by periodic boundaries. These boundary conditions eliminate inhomogeneities (Thornton, 2000; Huang *et al*, 2014a). The particle size distribution (PSD) used for all simulations is representative of Toyoura sand (Figure 1). A simplified Hertz-Mindlin contact model was used. The input parameters were a shear modulus (G) of 29 GPa, particle Poisson's ratio (ν) of 0.12, particle density (ρ) of 2650 kg/m^3 and local damping coefficient of 0.1. Initially, the periodic cell was deformed until the system reached an isotropic stress state with an initial mean effective stress (p'_0) of 25 kPa. After reaching the desired p'_0, the system was subjected to numerical cycling until p' and the number of contacts became constant indicating equilibrium. Ten samples were created and the initial void ratio of each sample was controlled using different inter-particle friction coefficients (μ) during the isotropic compression stage, as indicated in Table 1.

Once the isotropic compression stage had been finished, μ was set to 0.25 (Huang *et al*, 2014b). One-dimensional compression was then simulated by deforming the periodic cell: the top boundary was moved at a constant velocity in the vertical direction while the horizontal and bottom boundaries were maintained in a fixed position. The velocity chosen was sufficiently small to ensure that the system was maintained in the quasi-static regime (i.e., inertial number (I) $\leq$ 2.5e-3) (MiDi, 2004; da Cruz, 2005). The stresses in the periodic cell were determined using the particle and contact force data (Bagi, 1996; Potyondy & Cundall, 2004). Ten triaxial tests were carried out to define the $e_0 - \phi'_p$ relationship and obtain ϕ'_{cv} for the simulated sand. Details of the triaxial simulations and corresponding results are shown in Table 2.

3. Results

3.1. Macro response

Results from six representative one-dimensional compression tests are plotted in Figure 2. The initial void ratios at the start of compression ranged from e_0 = 0.544 as the densest sample to e_0 = 0.664 corresponding to the loosest of these six samples. Tests were terminated at mean effective stress (p')

values between 750 and 950 kPa. Referring to Figure 2(a), the effective stress ratio (q/p') decreased as e_0 increased. Figure 2(b) indicates that the axial strain level (ε_1) at which a given value of q was reached increased with e_0. For the densest sample (e_0 = 0.544), q = 100 kPa was achieved at $\varepsilon_1 \approx$ 0.07%, while for the loosest sample ε_1 exceeded 0.25% at the same q level. Figure 2 also includes results from laboratory tests from Chu & Gan (2004) and Wanatowski & Chu (2007), which indicate that the observations from the simulations are qualitatively consistent with the experimental data.

The horizontal stresses were calculated as the mean value of σ'_x and σ'_y. Figure 3(a) illustrates the variation of K_0 with effective vertical stress (σ'_v), while Figure 3(b) illustrates the variation in K_0 with the major principal strain (ε_1) (i.e., the vertical strain); both sets of data illustrate a clear dependency of K_0 upon e_0. Generally, loose samples attained higher K_0 values than denser samples, in line with previous experimental observations by Chu & Gan (2004), Wanatowski & Chu (2007) and Okochi & Tatsuoka (1984) that are included in Figure 3 for comparison. Interestingly, while different preparation methods were used in the experimental studies, i.e., as air pluviation (Okochi & Tatsuoka, 1984) or moist tamping (Chu & Gan, 2004, Wanatowski & Chu, 2007) and different initial stress conditions were applied, the trend is more or less the same for all the experiments and DEM simulations. Note that K_0 did not reach a constant value when plotted either against either σ'_v or ε_1 but decreased continuously for all samples, indicating that K_0 depends on σ'_v and ε_1.

Figure 4(a) shows the variation of K_0 with initial void ratio at three discrete values of σ'_v while Figure 4(b) gives K_0 at three discrete ε_1 values. For each value of σ'_v or ε_1 considered, the relationship between K_0 and void ratio can be represented by a power law equation. Laboratory data in terms of K_0 and e_0 were collected and plotted in Figure 4 for comparison. The dashed lines correspond to Jaky's equation used by Wanatowski & Chu (2007) from plane-strain and triaxial tests. Generally, K_0 values obtained in the DEM simulations and laboratory tests increase with increasing e_0. A power law relationship between K_0 and e_0 is identified for numerical data. This relationship differs from the linear K_0-e_0 relationship observed and proposed by Chu & Gan (2004) and Wanatowski & Chu (2007) for loose marine sand samples prepared by moist tamping (MT) and water sedimentation (WS) methods. Results from Hendron (1963) indicate a gentler linear increase of K_0 with e_0 for rounded Minnesota sand. A steeper response was found for Toyoura sand as reported by Okochi & Tatsuoka (1984). The K_0 values for Toyoura sand are closer to those from the numerical tests than other types of sand. Figure 4(a) illustrates a similar dependency of K_0 on σ'_v observed by Okochi & Tatsuoka (1984). The differences between the magnitudes of K_0 for the physical sands tested and for the numerical simulations can be attributed to particle size, shape (perfect spheres, angular and sub-angular sands) and differences in initial anisotropies (Guo & Stolle, 2006). It is important to note, however, that in the current study the structural anisotropy is induced entirely by the strain path

imposed, while in the experimental studies, there will be an initial anisotropic structure as a consequence of gravity deposition during sample preparation.

Figure 4(c) compares the measured K_0 values with the predicted K_0 from Jaky's equation using ϕ'_p, ϕ'_{cv} and the angle of shearing resistance mobilized during the 1D compression tests (ϕ'_{mob}), calculated from $\sin \phi'_{mob} = (\sigma'_v - \sigma'_h)/(\sigma'_v + \sigma'_h)$ at the same discrete values of σ'_v where K_0 was directly measured. From the triaxial results shown in Table 2, an exponential relationship between ϕ'_p and e_0 as observed by Wanatowski & Chu (2006) is evident and thus the K_0- e_0 relationship is established. For the case of σ'_v = 700 kPa, Jaky's equation overestimates the K_0 values for dense samples (e_0< 0.65) by as much as 0.12 considering ϕ'_p as input for Jaky's formula, while for looser samples (e_0> 0.65), K_0 is underestimated by up to 0.05 when ϕ'_{cv} is used. Similar findings are presented by Wanatowski & Chu (2007) as indicated in Figure 4(a) which are consistent with how Jaky (1944) derived Equation (1), by considering a normally consolidated mass of soil in a loose condition and thus giving better predictions for loose states when considering ϕ'_{cv}. The data points calculated for K_0 using ϕ'_{mob} in Jaky's equation are located above those measured in the numerical simulations. Considering that the ratio of horizontal to vertical stresses can be expressed as $(1 - \sin \phi'_{mob})/ (1 + \sin \phi'_{mob})$, applying ϕ'_{mob} in Jaky's equation would displace the predicted values from those measured. The variance of the numerical K_0 is in line with those reported from laboratory experiments. This can be observed in Figure 5 which shows K_0 against ϕ'_{cv} for a range of soils including sands and clays as summarized by Wood (1990) based on results from Wroth (1972) and Ladd *et al* (1977). Jaky's equation is included in Figure 5 where it can be observed how the experimental results are enclosed between -0.20 and +0.12 from Jaky's equation with the numerical results also falling between those limits.

3.2 Micro scale analysis

Prior authors have attributed the K_0 dependency on void ratio to the different internal fabrics formed during sample preparation (Wanatowski & Chu, 2007; Lee *et al*, 2013). However, these relationships are hypothetical as the material fabric cannot be directly quantified in conventional laboratory tests. The DEM simulation data provide information on the direction of contacts. Satake (1982) proposed quantifying structural (fabric) anisotropy using the fabric tensor, which is defined as:

$$\Phi_{ij} = \frac{1}{N_c} \sum_1^{N_c} n_i n_j \quad (2)$$

where N_c is the total number of contacts and n_i is the unit contact normal. The largest, intermediate and smallest eigenvalues of the fabric tensor are denoted as Φ_1, Φ_2, and Φ_3 respectively. The ratio between Φ_3 and Φ_1 can be adopted to describe the degree of structural anisotropy: $F = \Phi_3/\Phi_1$, with the condition of $\Phi_3 = \Phi_2$ being closely satisfied. F equalling to zero represents the highest degree of structural anisotropy while F equalling to one indicates an isotropic state. Figures 6(a) and 6(b) show

the evolution of the normalized F (F/F_0) with σ'_v and ε_1, respectively, where F_0 is the degree of structural anisotropy after isotropic compression and is in the range of 0.9904 to 0.9961. Figure 6(a) indicates that F/F_0 decreases as σ'_v increases. Dense samples attained lower values of F/F_0 than looser samples, and as Figure 6(b) shows, dense samples also showed a more rapid decrease in F/F_0 than looser samples during straining. Figure 6(c) plots K_0 against F/F_0 (up to $\varepsilon_1 = 0.25\%$), from which it is evident that K_0 values increase as F/F_0 values increase for all the packing densities considered. In general, while dense samples showed a higher degree of anisotropy, loose samples remained more isotropic. It is also noticeable that while K_0 decreases with σ'_v, the degree of structural anisotropy increases with σ'_v.

Rothenburg & Bathurst (1989) analytically showed that the stress ratio is related to different sources of anisotropy, including geometrical anisotropy, normal contact force anisotropy and tangential contact force anisotropy, of which the normal contact force anisotropy (a_n) dominates. It is worth exploring the K_0 - a_n relationship for the DEM simulations. The definition of a_n follows Rothenburg & Bathurst (1989) and Guo & Zhao (2013) with the average normal contact force tensor expressed by Equation (3) (where Φ'_{ij} is the deviatoric part of Φ_{ij}) with its probability distribution given by Equation (4) and $a_{ij}^n = (15/2)F_{ij}'^n / \bar{f}^0 . \bar{f}^0 = F_{ii}^n$ is the average normal contact force calculated considering the entire Ω, different from the mean normal contact force averaged over all contacts. a_n is related to the second invariant of a_{ij}^n as $a_n = \sqrt{(3/2)a_{ij}^n a_{ij}^n}$.

$$F_{ij}^n = \frac{1}{4\pi}\int_\Omega \bar{f}_n(\Omega) n_i n_j d\Omega = \frac{1}{N_c}\sum_1^{N_c} \frac{f_n n_i n_j}{1+(15/2)\Phi_{ij} n_k n_l} \quad (3)$$

$$\bar{f}_n(\Omega) = \bar{f}^0[1+a_{ij}^n] \quad (4)$$

Figures 7(a) and 7(b) indicate the evolution of a_n with σ'_v and ε_1, respectively. There is a clear influence of the initial void ratio with denser samples attaining higher values of a_n than looser ones. Figure 7(b) shows that all samples have attained an almost constant value of a_n after 0.05% of ε_1. Figure 7(c) plots K_0 against a_n, where a similar path is noticed for all the samples.

The relationships between K_0 and F/F_0 at different values of σ'_v and ε_1 are presented in Figure 8(a) and 8(b). In both cases, and for all stages, a linear relationship can be found between K_0 and F/F_0 in which higher values of K_0 are always related to higher F/F_0. The relationships between K_0 and a_n at different values of σ'_v and ε_1 are presented in Figure 8(c) and 8(d). Regardless of stress or strain levels, the relationship between K_0 and a_n can be represented by a single line that shows lower values of K_0 at higher a_n.

For a clearer illustration of the influence of structural anisotropy and normal contact force anisotropy, Figures 9(a) and 9(b) present the contact rose diagrams for a dense (test K0-1) sample and a loose

(test K0-9) sample at the same level of σ'_v considering the projections onto the *x-z* vertical plane using an angular increment of 10 degrees. The radial length of each bin indicates the number of contacts oriented within the angle defining the bin. The colour of each bin is proportional to the sum of the normal contact forces that are present in that bin. For the dense sample, the stronger contacts that carry higher forces are preferentially aligned in the loading (i.e., vertical) direction, while the weaker contacts (transmitting lower force) tend to be oriented orthogonal to the loading direction. A larger number of contacts are present in the vertical direction than in the horizontal direction leading to lower values of *F*. More stress is transmitted in the vertical direction than in the horizontal direction, resulting in a larger value of σ'_v and a smaller value of σ'_h. The loose sample presents a more isotropic distribution of both contact direction and force magnitude, yielding higher values of *F*. Moreover, contact forces transmitted in the horizontal direction are closer in magnitude to those transmitted in the vertical direction, making the values of σ'_v and σ'_h more alike. This explains why K_0 values decrease with increasing packing density.

4. Conclusions

One-dimensional tests on initially isotropic samples with a range of void ratios have been simulated using DEM. The resulting dependency of K_0 on void ratio qualitatively agrees with previously published laboratory tests, i.e., K_0 increases as void ratio increases. A power-law relationship between K_0 and e_0 was observed and this relationship depends on the stress level and vertical strain. Three definitions of ϕ' were considered when applying Jaky's expression (ϕ'_{mob}, ϕ'_p and ϕ'_{cv}) and compared to the measured K_0. While the use of ϕ'_p gave the best match at lower void ratios and ϕ'_{cv} reported fair predictions for looser samples, none of these expressions gave a good match with the measured K_0 values for the entire range of void ratio and stress levels considered. Micro-scale analysis revealed that the variation of K_0 with void ratio is related to the degree of both structural anisotropy and normal contact force anisotropy. K_0 decreases linearly with increasing structural anisotropy quantified using the ratio of major and minor principal values of the fabric tensor, *F*. The K_0- *F* relationship was seen to depend on stress and strain level while a unique relationship, independent of stress or strain level, was found between K_0 and a_n. Dense samples had higher degrees of structural and normal contact force anisotropy at all test stages while loose samples remained more isotropic with lower normal contact force anisotropy. Loose samples were found to transmit similar stresses in all directions, while for dense samples, stress transmission coincides preferentially with the vertical loading direction. Therefore, K_0 values for dense samples are smaller than those of loose samples. The results of this study support the hypothesis of Lee *et al* (2013) and Wanatowski & Chu (2007) that K_0 values are related to the internal structure.

Acknowledgements

The work presented in this study was supported and financed by The University of Hong Kong. Mr. Lopera would like to thank the IT Department at The University of Hong Kong for providing access to the high performance computer HPCPOWER2 in order to conduct the simulations presented in this work. The suggestions from the anonymous referees that helped improve the content of the paper are also acknowledged.

References

Bagi, K. (1996). Stress and strain in granular assemblies. *Mech. Mater.* 22, 165-177.

Been, K. and Jefferies, M. G. (1985). A state parameter for sands. *Géotechnique* 35, No. 2, 99 – 112.

Chu, J. & Gan, C. L. (2004). Effect of void ratio on K_0 of loose sand. *Géotechnique* 54, No. 4, 285-288.

da Cruz F., Emam S., Prochnow M., J. N. Roux and F. Chevoir (2005). Rheophysics of dense granular materials: Discrete simulation of plane shear flows. *Phys. Rev.* E, 72, 021309

Guo N. and Zhao J. (2013). The signature of shear-induced anisotropy in granular media. *Comput. Geotech.* 47, 1 – 15

Guo P. J. and Stolle D. F. E. (2006). Fabric and particle shape influence on K_0 of granular materials. *Soils Found.* 46 No. 5, 639-652.

Hendron A. J. (1963). The behaviour of sand in one-dimensional compression. *PhD Thesis, University of Illinois at Urbana Champaign, Urbana*.

Huang, X., Hanley, K. J., O'Sullivan, C. & Kwok, C.Y. (2014a). Effect of sample size on the response of DEM samples with a realistic grading. *Particuology*, 15, 107-115.

Huang, X., Hanley, K. J., O'Sullivan, C. & Kwok, C.Y. (2014b). Exploring the influence of interparticle friction on critical state behaviour using DEM. *Int. J. Numer. Anal. Met.* 38 No. 12, 1276-1297.

Jaky, J. (1944). The coefficient of earth pressure at rest. In Hungarian (A nyugalmi nyomas tenyezoje). *J. Soc. Hung. Eng. Arch.* 78 No. 22, 355-358.

Ladd, C.C., Foott, R., Ishihara, K., Schlosser, F., and Poulus, H.G. (1977), 'Stress-deformation and strength characteristics', in Proc. 9th Int. Conf. on Soil Mechs and Foundation Eng., Tokyo (Tokyo: Japanese Society of Soil Mechanics and Foundation Engineering), vol. 2, pp. 421 – 94.

Lee, J., Yun, T. S., Lee, D., & Lee. J. (2013). Assessment of K_0 correlation to strength for granular materials. *Soils Found.* 53 No. 4, 584-595.

Mesri, G and Hayat, T.M. (1993). Coefficient of earth pressure at rest. *Can. Geotech. J.* 30, 647 – 666.

Mesri, G. & Vardhanabhuti, B. (2007). Coefficient of earth pressure at rest for sands subjected to vibration. *Can. Geotech. J.* 44, 1242-1263.

MiDi G. D. R. (2004). On dense granular flows. *Eur. Phys. J E* 14, 341 – 365.

Northcutt S. and Wijewickreme D. (2013). Effect of particle fabric on the coefficient of lateral earth pressure observed during one-dimensional compression of sand. *Can. Geotech. J.* 50, 457-466.

Okochi Y. and Tatsuoka F. (1984). Some factors affecting K_0 – values of sand measured in triaxial cell. *Soils Found.* 24 No. 3, 52-68.

Plimpton, S. (1995). Fast parallel algorithms for short-range molecular dynamics. *J. Comput. Phys.* 117, 1-19.

Potyondy D. O. and Cundall P. A. (2004). A bonded-particle model for rock. *Int J Rock Mech Min.* 41, 1329 – 1364.

Rothenburg L. and Bathurst R. J. (1989). Analytical study of induced anisotropy in idealized granular materials. *Géotechnique* 39, No. 4, 601 – 614.

Satake, M. (1982). Fabric tensor in granular materials. In *Deformation and failure of granular materials* (eds P. A. Vermeer and H. J. Luger), pp. 63-68. Rotterdam: Balkema.

Talesnick, M. L. (2012). A different approach and result to the measurement of K_0 of granular materials. *Géotechnique* 62, No. 11, 1041-1045.

Thornton, C. (2000). Numerical simulations of deviatoric shear deformation of granular media. *Géotechnique* 50, No. 1, 43-53.

Wanatowski, D. and Chu J. (2006). Stress-strain behaviour of a granular fill measured by a new plane-strain apparatus. *Geotech. Test J.* 29, No. 2, 149-157.

Wanatowski, D. and Chu J. (2007). K_0 of sand measured by a plane-strain apparatus. *Can. Geotech. J.* 44, 1006-1012.

Wood D. M. (1990). Soil behaviour and critical state soil mechanics. *Cambridge University Press.*

Wroth, C.P. (1972). General theories of earth pressure and deformation, in Proc. 5th European Conf. on Soil Mechs and Foundation Eng., Madrid (Madrid: Sociedad Española de Mecanica de Suelo y Cimentaciones), vol 2, pp. 33 – 52.

Notation

a_n	Normal contact force anisotropy.
e	Void ratio
F	Structural anisotropy ($F = \Phi_3/\Phi_1$)
F_0	Structural anisotropy after isotropic compression

F_{ij}^{n}	Average normal contact force tensor
$\overline{f}_{n}(\Omega)$	Probability distribution of the average normal contact force tensor
G	Particle shear modulus
I	Inertial number
K_0	Coefficient of lateral earth pressure at rest
p'	Mean effective stress
p'_0	Mean effective stress after isotropic compression
q	Deviatoric stress
ε_1	Major principal strain
μ	Inter-particle friction coefficient
v	Particle Poisson's ratio
ρ	Particle density
σ'_h	Horizontal effective stress ($\sigma'_h = 0.5(\sigma'_x + \sigma'_y)$)
σ'_v	Vertical effective stress ($\sigma'_v = \sigma'_z$)
Φ_{ij}	Fabric tensor
Φ_1; Φ_2; Φ_3	Major, intermediate and minor components of the fabric tensor (Φ_{ij}).
ϕ';ϕ'_p; ϕ'_{mob}; ϕ'_{cv}	Effective angle of shearing resistance, peak angle of shearing resistance, mobilized angle of shearing resistance and critical state angle of shearing resistance.

Figures and Tables

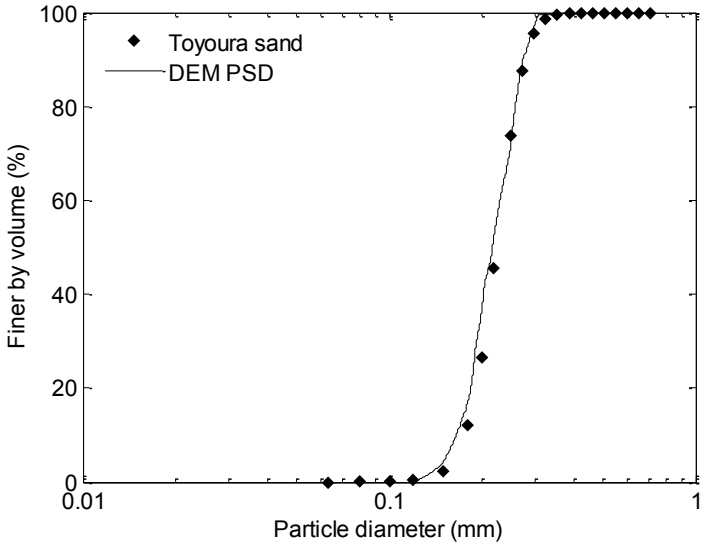

Figure 1. Particle size distribution of numerical samples compared with laboratory data for Toyoura sand.

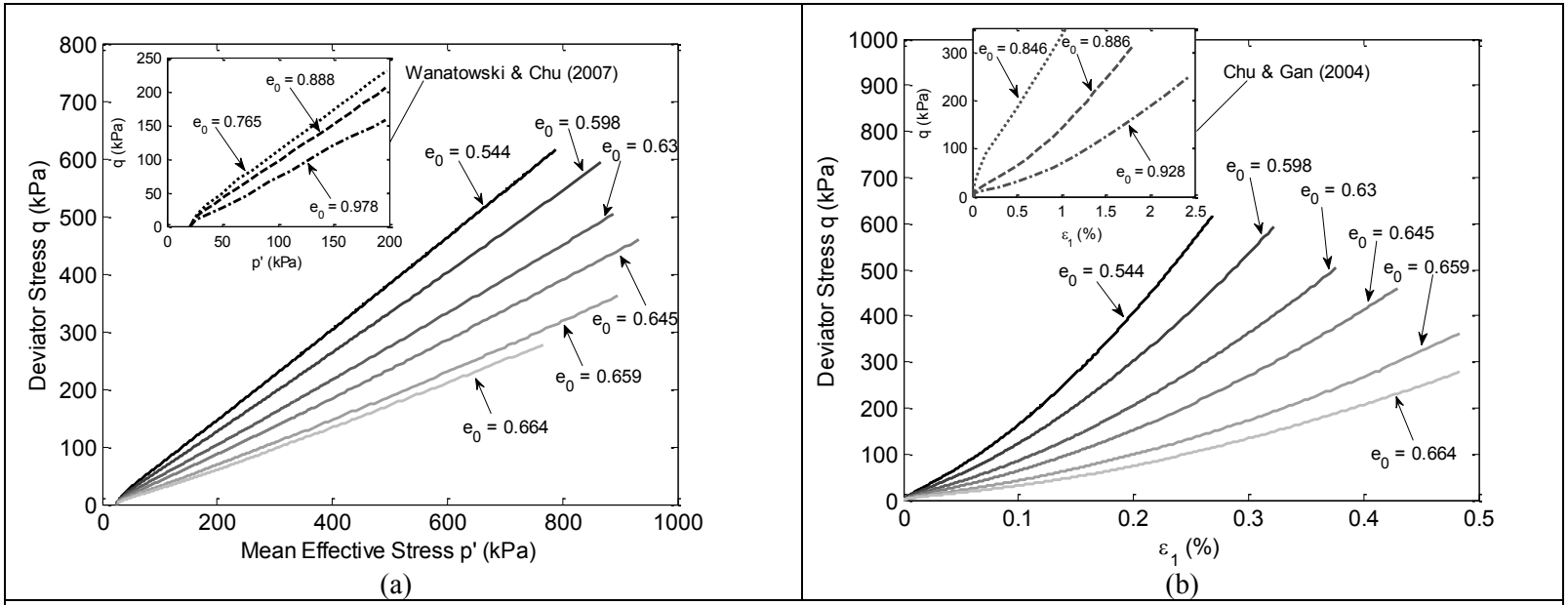

Figure 2. Results from K_0 tests. (a) Effective stress paths q Vs p', (b) Stress – strain curves q Vs ε_1 (Experimental data after Wanatowski & Chu (2007) and Chu & Gan (2004) are presented in the inset subfigures).

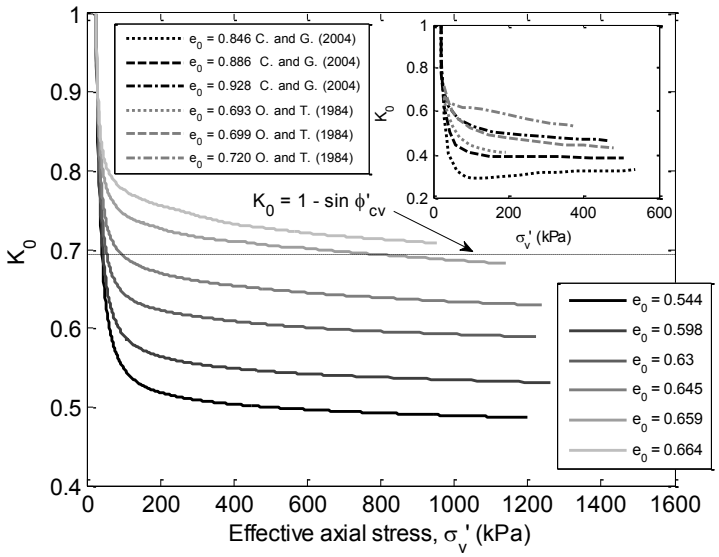

(a)

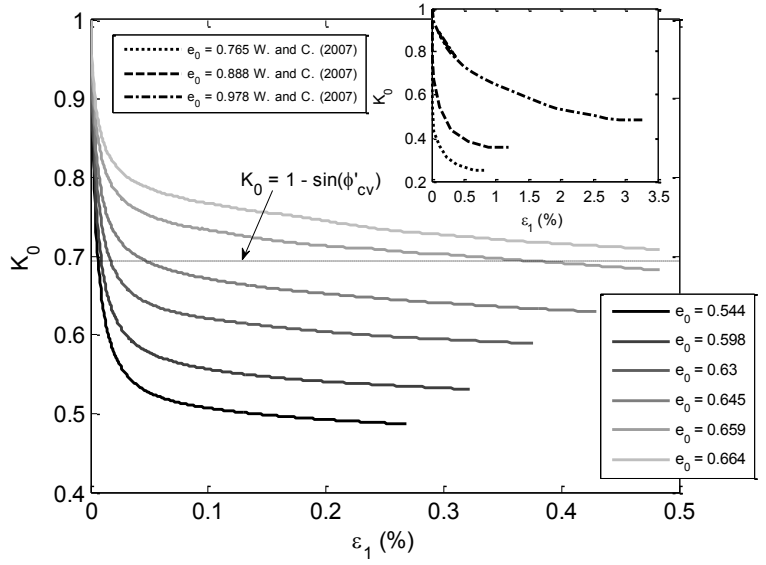

(b)

Figure 3. Results from K_0 tests. (a) K_0 Vs σ'_v (b) K_0 Vs ε_1, (Experimental data after Chu & Gan (2004), Okochi & Tatsuoka (1984) and Wanatowski & Chu (2007) are presented in the inset subfigures).

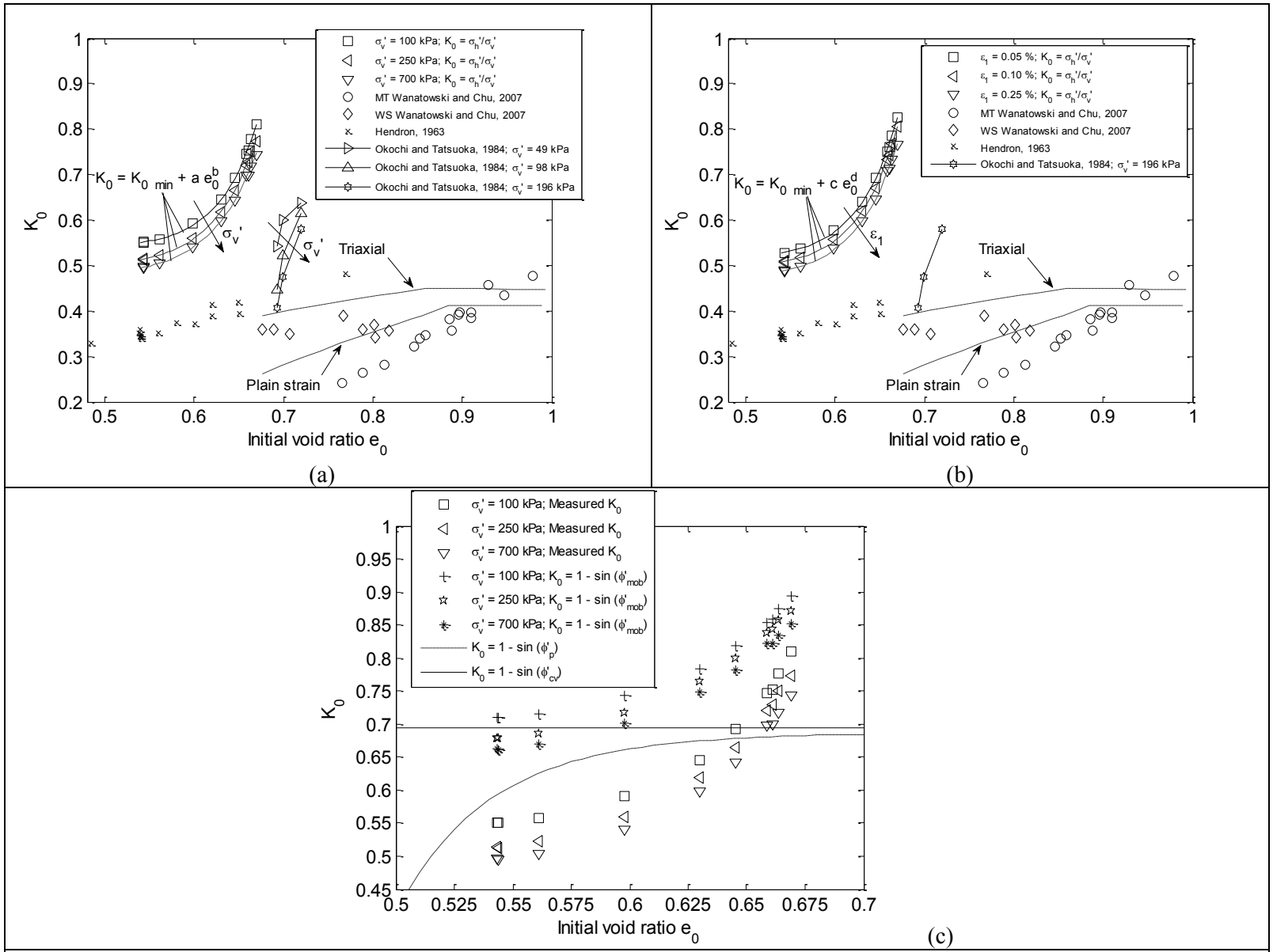

Figure 4. K_0 against void ratio. (a) At different levels of σ'_v and (b) At different stages of ε_1. Experimental data after Hendron (1963), Okochi & Tatsuoka (1984) and Wanatowski & Chu (2007). (c) Measured K_0 at different levels of σ'_v and predicted values applying ϕ'_{mob}, ϕ'_p and ϕ'_{cv} into Jaky's equation.

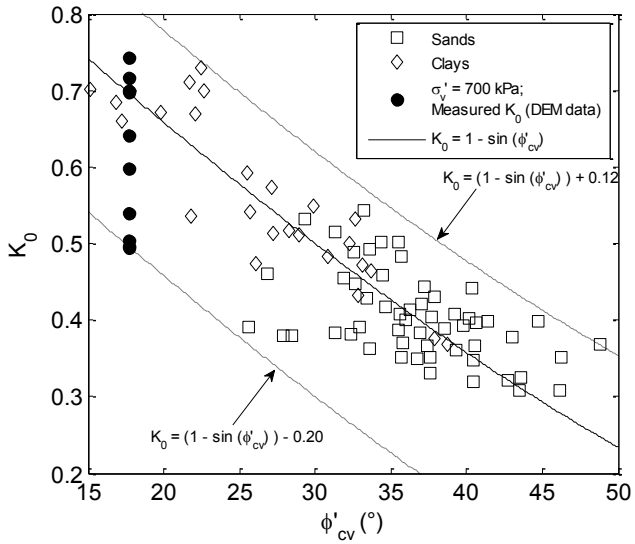

Figure 5. Experimental data of K_0 for normally compressed soils together with numerical data from this study. Experimental data after Wroth (1972) and Ladd et al (1977).

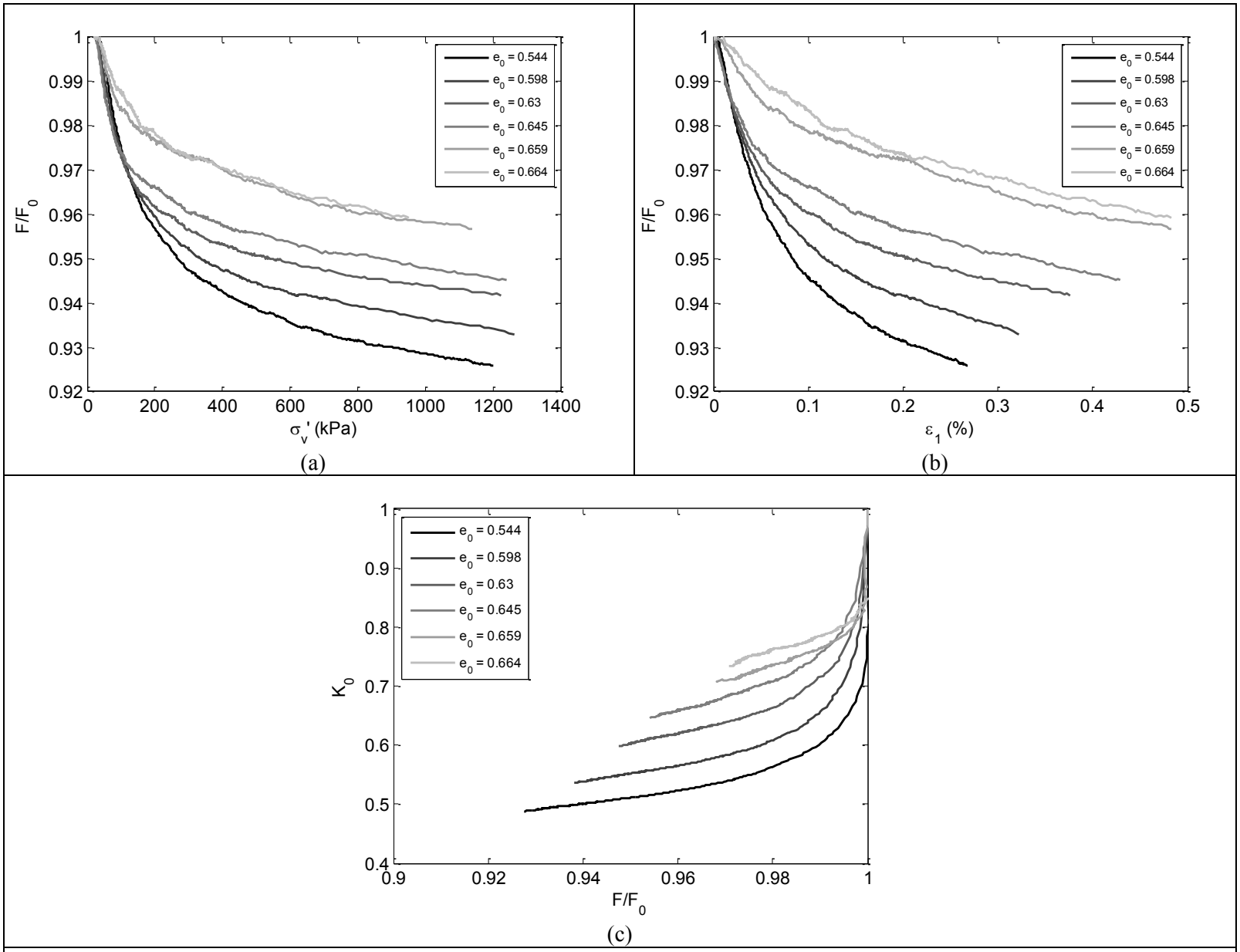

Figure 6. Normalized degree of structural anisotropy. (a) F/F_0 against σ'_v, (b) F/F_0 against ε_1 and (c) K_0 against F/F_0.

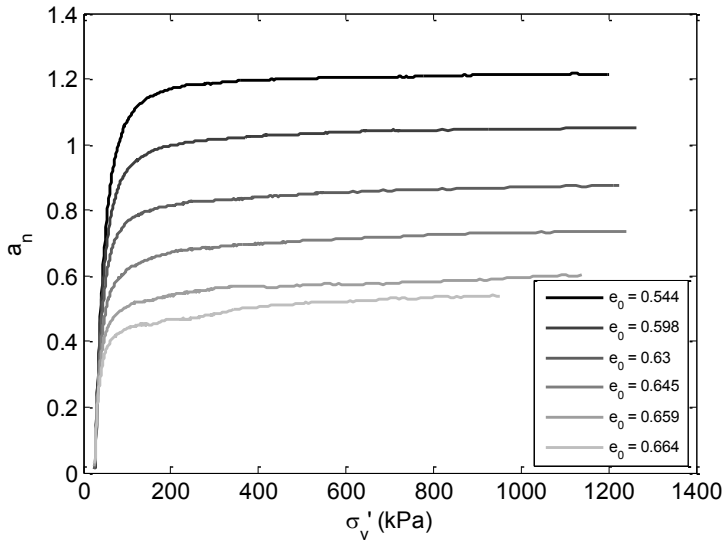

(a)

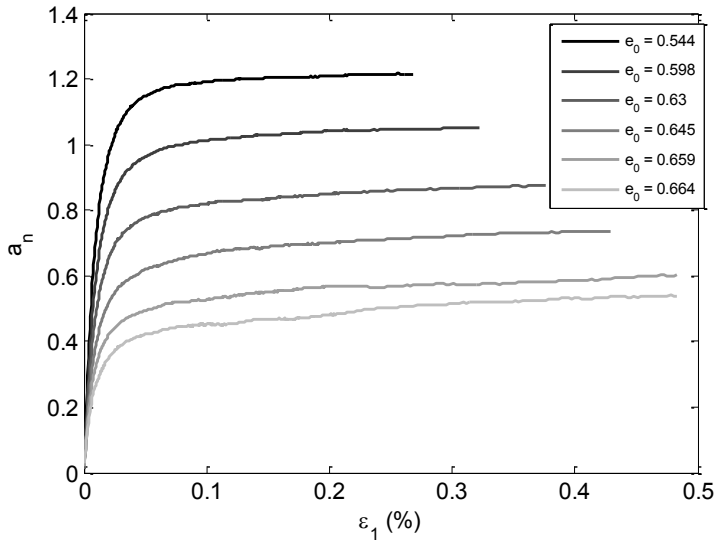

(b)

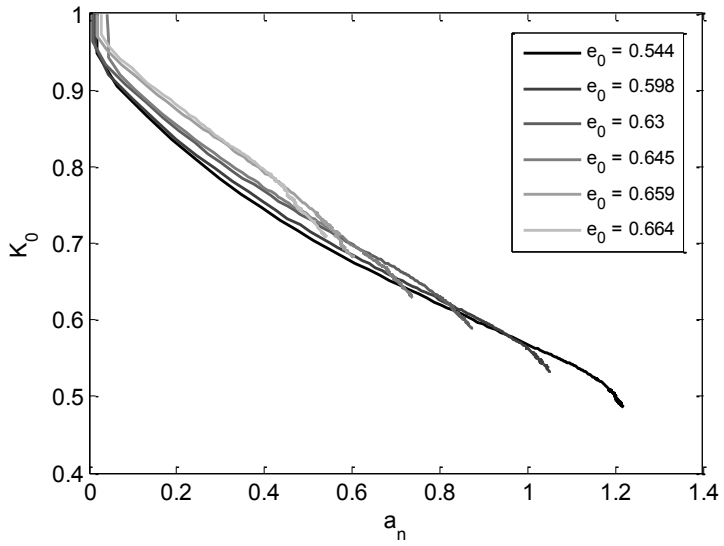

(c)

Figure 7. Normal contact force anisotropy. (a) a_n against σ'_v, (b) a_n against ε_1 and (c) K_0 against a_n.

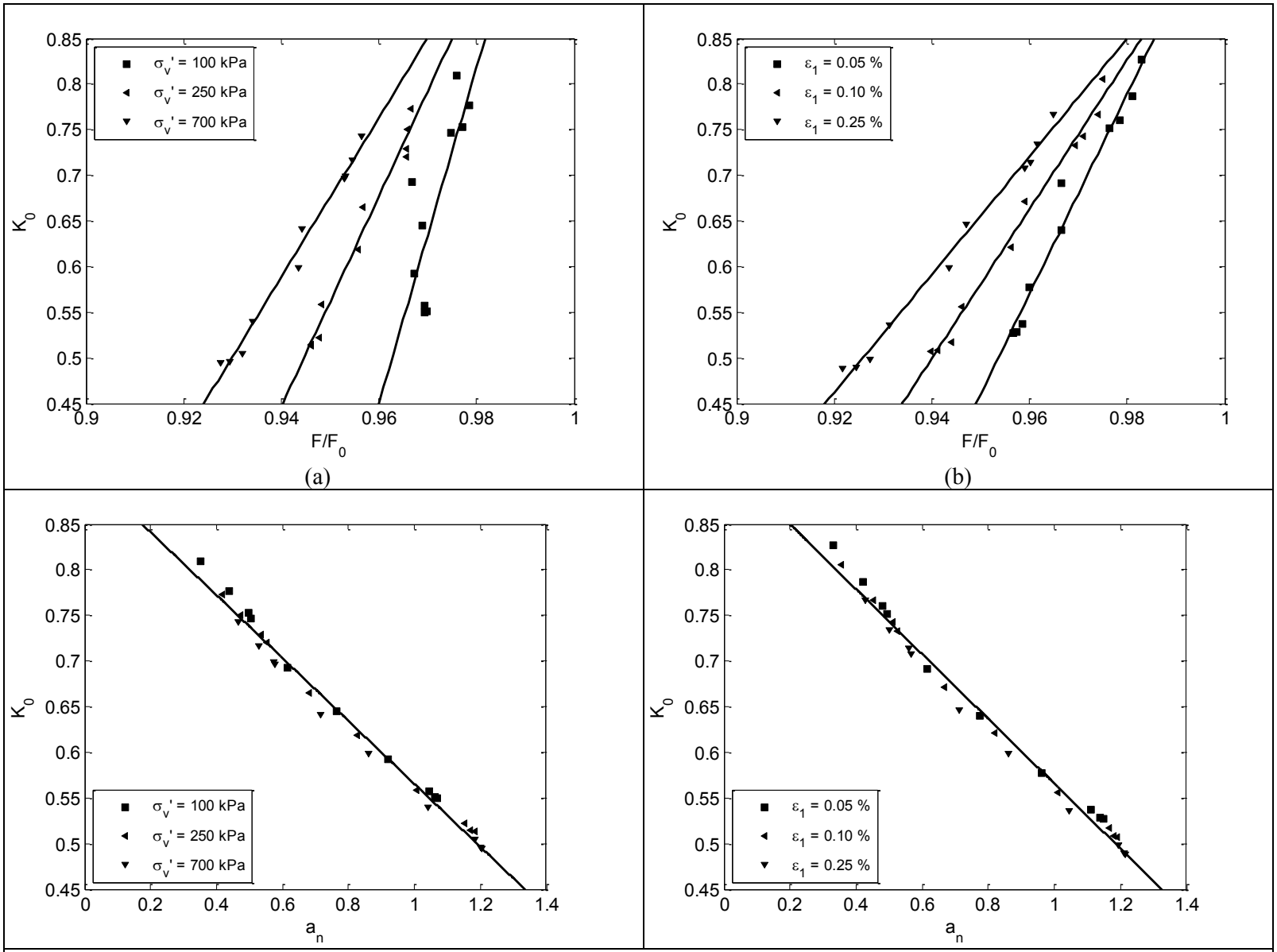

Figure 8. K_0 against F/F_0. (a) At different σ'_v and (b) different stages of ε_1 and K_0 against a_n. (c) At different σ'_v and (d) different stages of ε_1

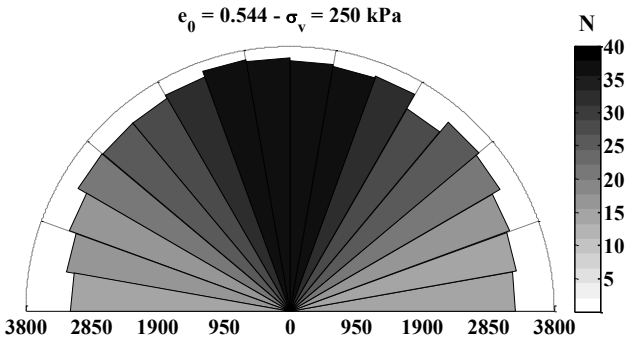

(a)

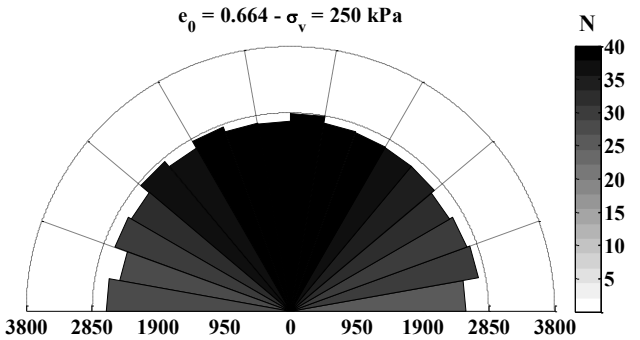

(b)

Figure 9. Comparison of contact rose diagrams at the same value of σ'_v for (a) a dense sample and (b) a loose sample.

Table 1. Summary of numerical K_0 tests conducted

Test ID	μ during isotropic compression	e_0 (after isotropic compression)
K0-1	5.0e-4	0.544
K0-2	1.0e-3	0.543
K0-3	1.0e-2	0.561
K0-4	5.0e-2	0.598
K0-5	0.11	0.630
K0-6	0.15	0.645
K0-7	0.19	0.659
K0-8	0.20	0.661
K0-9	0.215	0.664
K0-10	0.235	0.669

Table 2. Summary of data from triaxial simulations

Test ID	e_0	p_0' (kPa)	ϕ'_p (°)	ϕ'_{cv} (°)
TX-CD-100-0.5928	0.5928	100	20.10	17.82
TX-CD-500-0.5533	0.5533	500	22.73	
TX-CD-500-0.6059	0.6059	500	19.65	
TX-CD-500-0.6142	0.6142	500	19.21	
TX-CD-500-0.6615	0.6615	500	17.82	
TX-CD-1000-0.6142	0.6142	1000	19.00	
TX-CD-2500-0.5781	0.5781	2500	20.80	
TX-CD-5000-0.6482	0.6482	5000	17.82	
TX-CV-500-0.6238	0.6238	500	19.27	
TX-CV-500-0.6280	0.6280	500	19.13	